The adsorption mechanisms of organic micropollutants on high-silica zeolites causing S-shaped adsorption isotherms

An experimental and Monte Carlo simulation study

Jiang, Nan; Erdös, Mate; Moultos, Othon; Shang, Ran; Vlugt, Thijs J.H.; Heijman, Sebastiaan G.J.; Rietveld, Luuk C.

DOI
10.1016/j.cej.2019.123968

Publication date
2020

Document Version
Final published version

Published in
Chemical Engineering Journal

Citation (APA)
Jiang, N., Erdös, M., Moultos, O., Shang, R., Vlugt, T. J. H., Heijman, S. G. J., & Rietveld, L. C. (2020). The adsorption mechanisms of organic micropollutants on high-silica zeolites causing S-shaped adsorption isotherms: An experimental and Monte Carlo simulation study. *Chemical Engineering Journal*, *389*, 1-9. Article 123968. https://doi.org/10.1016/j.cej.2019.123968

Chemical Engineering Journal 389 (2020) 123968

Contents lists available at ScienceDirect

Chemical Engineering Journal

journal homepage: www.elsevier.com/locate/cej

The adsorption mechanisms of organic micropollutants on high-silica zeolites causing S-shaped adsorption isotherms: An experimental and Monte Carlo simulation study

Nan Jiang[a,*,1], Máté Erdős[b,1], Othonas A. Moultos[b,*], Ran Shang[a], Thijs J.H. Vlugt[b], Sebastiaan G.J. Heijman[a], Luuk C. Rietveld[a]

[a] Section of Sanitary Engineering, Department of Water Management, Faculty of Civil Engineering and Geosciences, Delft University of Technology, Stevinweg 1, 2628CN Delft, The Netherlands

[b] Engineering Thermodynamics, Process & Energy Department, Faculty of Mechanical, Maritime and Materials Engineering, Delft University of Technology, Leeghwaterstraat 39, 2628CB Delft, The Netherlands

HIGHLIGHTS

- TCP adsorption on high-silica FAU zeolites gives S-shaped isotherms.
- FAU zeolites with higher Si/Al ratio have more pronounced S-shaped isotherms.
- The S-shaped isotherm originate from the π-π interaction of TCP molecules.
- Water molecules inhibit the TCP adsorption in the supercages of FAU zeolites.

GRAPHICAL ABSTRACT

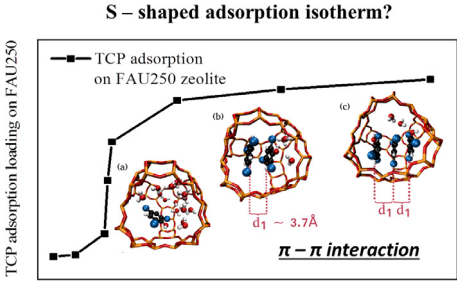

ARTICLE INFO

Keywords:
High-silica zeolites
Organic micropollutants
Monte Carlo simulation
S-shaped adsorption isotherms

ABSTRACT

The adsorption of organic micropollutants (OMPs) on high-silica zeolites is characterized by adsorption isotherms with various shapes. The occurrence of an S-shaped adsorption isotherm indicates the lack of adsorption affinity for OMPs at low, environmentally relevant equilibrium concentrations. In this study, S-shaped isotherms were observed during batch experiments with 2,4,6-trichlorophenol (TCP) and FAU zeolites. This is the first time that an S-shaped isotherm is reported for the adsorption of OMPs on high-silica zeolites. Monte Carlo (MC) simulations in the grand-canonical ensemble were used to obtain a better understanding of the mechanism of the S-shaped adsorption isotherms. From the MC simulation results, it was observed that multiple TCP molecules were adsorbed in the supercages of the FAU zeolites. It was found that the π-π interactions between TCP molecules give rise to the adsorption of multiple TCP molecules per supercage, and thus causing an S-shaped adsorption isotherm. Simulations also revealed that water molecules were preferentially adsorbed in the supercages and sodalite cages of the FAU zeolites. FAU zeolites with a higher Al content adsorbed a higher amount of water molecules and a lower amount of TCP, and showed less pronounced S-shaped isotherms.

* Corresponding authors.
E-mail addresses: n.jiang@tudelft.nl (N. Jiang), o.moultos@tudelft.nl (O.A. Moultos).
[1] Nan Jiang and Máté Erdős contributed equally to this work.

https://doi.org/10.1016/j.cej.2019.123968
Received 13 November 2019; Received in revised form 23 December 2019; Accepted 26 December 2019
Available online 27 December 2019

1. Introduction

Zeolites are crystalline, microporous aluminosilicates with a well-defined 3-dimensional structure, composed of tetrahedral SiO_4 and AlO_4 clusters connected to each other by shared oxygen atoms. To compensate the charge imbalance caused by the Al content of the framework, exchangeable cations (usually alkali and alkaline earth cations) are located in the cavities of the structure. Due to these intrinsic characteristics, e.g. exchangeable cations and a well-defined pore structure, zeolites are widely used as catalysts, molecular sieves, and adsorbents for air-pollution remediation, gas separation and removal of volatile organic compounds [1–6].

An important characteristic of zeolites is the ratio of the Si and Al atoms contained. This ratio determines the level of hydrophobicity in the framework. Based on the Si to Al molar ratio, three types of zeolites can be identified, the low-silica (i.e., Si/Al $<$ 2), the medium-silica (i.e., Si/Al = 2 – 5) and the high-silica (i.e., Si/Al $>$ 5) [7,8]. Low- and medium-silica zeolites exhibit a high ion exchange capability and are widely applied as water hardness control ingredients in detergents [9]. High-silica zeolites are particularly useful for removal of organic micropollutants (OMPs) from water, since their hydrophobic nature promotes the adsorption of OMPs instead of water [10–12]. As the framework type of the zeolite defines its unique structural features, including pore opening sizes, and cage and channel structures, it highly affects the adsorption efficiency of OMPs [13,14]. Various families of commercially available high-silica zeolites, including the Faujasite (FAU), Mordenite (MOR), Beta (BEA) and ZSM-5 (MFI) types, have been shown to be effective adsorbents for OMP removal from water [15–18].

In the process of OMP adsorption from water on solid adsorbents, the adsorption isotherm describes the relation between the equilibrium concentration of OMPs in water and the adsorption loading of OMPs on the solid adsorbents. Giles et al. [19] have divided the types of adsorption isotherms into the four groups shown in Fig. 1. The C-shaped adsorption isotherm (Fig. 1a) describes a linear increase of OMP adsorption loading with the equilibrium concentration of OMPs in water, which is often used for a narrow range of OMP concentrations or for very low OMP concentrations, i.e., from a few ng L^{-1} to several μg L^{-1} [20]. When the adsorbent has a limited number of adsorption sites, a plateau in the adsorption isotherm appears after a specific equilibrium concentration of OMPs and above, suggesting the saturation of the adsorbent. This results in the L-shaped (Fig. 1b) and H-shaped (Fig. 1c) isotherms. The steeper increase of OMP adsorption loading in the H-shaped isotherms compared to the L-shaped ones indicates that the zeolites exhibiting H-shaped isotherms have a higher affinity for OMPs.

In some adsorption processes, the isotherms exhibit a characteristic S-shape (Fig. 1d) [21]. This shape can be attributed to the higher attraction between OMPs at the surface of the adsorbent or to a complexation reaction of the metallic species of OMPs with ligands in water [20,22]. In general, the occurrence of S-shaped isotherms indicates the unfavorable OMP adsorption at low equilibrium concentrations.

Traditionally, the adsorption of OMPs on adsorbents are mostly obtained from batch experiments. It has been observed in several experimental studies that the adsorption of various OMPs from aqueous solutions on high-silica zeolites result in different types of adsorption isotherms. The adsorption of hydroxycinnamic acids, i.e., p-coumaric acid and ferulic acid, on high-silica zeolites were studied by Simon et al. [23]. At the equilibrium concentration range of 0 – 1 g L^{-1}, BEA zeolites showed H-shaped isotherms, while FAU zeolites gave L-shaped isotherms, indicating that BEA zeolites, having smaller pore sizes, have a higher affinity for the hydroxycinnamic acids than FAU zeolites. The plateaus in both isotherms have been attributed to the saturation of the micropores of the zeolites with hydroxycinnamic acids. Zhang et al. [24] studied 2,4,6 trichlorophenol (TCP) adsorption on FAU zeolites. At an equilibrium concentration of 0 – 30 mg L^{-1}, a C-shaped adsorption isotherm was obtained.

Although the adsorption experiments can be used to design or optimize zeolite-based adsorbents for the removal of OMPs from water, they do not provide any information on the exact adsorption mechanisms [25]. To that end, molecular simulation provides the necessary atomistic resolution needed to promote the deeper understanding of the governing physical–chemical mechanisms in adsorption equilibrium, and to further guide adsorption experiments. During the last three decades molecular simulations are actively performed in order to support experiments in various industrial and environmental processes [26–28]. In particular, Monte Carlo (MC) simulations with classical force fields have been used to study adsorption processes in porous media including metal–organic frameworks [29–31], zeolites [32–35], and activated carbon [36,37]. Due to the high interest in zeolite structures for adsorption-based applications in energy storage [38–40], gas separation [41,42], and wastewater treatment [43,44], numerous MC simulation studies have been carried out to explain the adsorption mechanisms of various compounds and mixtures [45–49].

2,4,6 trichlorophenol (TCP) is an organic compound widely used for the production of industrial products, e.g., fungicide and herbicide. As a result, TCP has been repeatedly reported to occur in water bodies [50–52] as an important OMP, among others. In the present work, the adsorption of TCP from water on high-silica FAU zeolites was studied by means of both adsorption experiments and MC simulation. FAU zeolites were chosen due to their large pore size and amount of micropores, which is shown to have a high adsorption loading for various OMPs [53–55]. The schematic representation of the framework of FAU is shown in Fig. 2.

In batch experiments of TCP adsorption on high-silica FAU zeolites, an S-shaped adsorption isotherm was obtained. To the best of our knowledge, this is the first time that an S-shaped isotherm has been reported for the adsorption of OMPs on high-silica zeolites. In this context, MC simulations were carried out to investigate the adsorption mechanisms of the occurring S-shaped isotherm. Moreover, this is also one of the very few MC simulation studies reporting the adsorption of organics from water on high-silica zeolites [58–60]. To understand the adsorption mechanism, causing the S-shaped adsorption isotherm, the experimentally measured and the computed adsorption isotherms were compared qualitatively. The relation between the amount of Al content in FAU zeolites and the occurrence of S-shaped isotherms was also discussed.

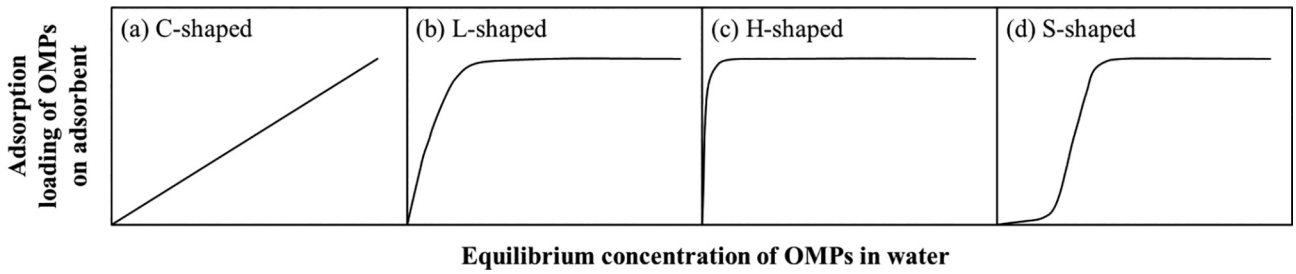

Fig. 1. The four characteristic types of adsorption isotherms as classified by Giles et al. [19]: (a) C-shaped, (b) L-shaped, (c) H-shaped, and (d) S-shaped.

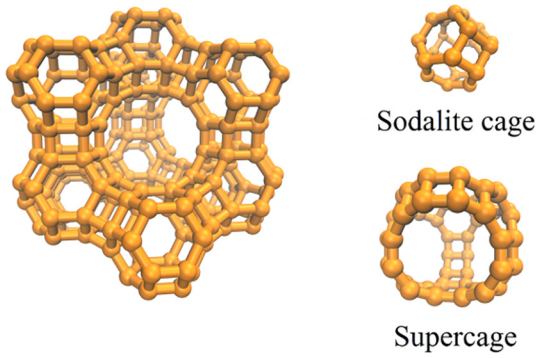

Fig. 2. The pores in FAU zeolites are made of supercages and sodalite cages with pore opening diameters 7.4 Å and 2.3 Å, respectively [56,57].

2. Materials and methods

2.1. Materials

TCP standards for chromatography analyses were purchased from Sigma-Aldrich, the Netherlands. The basic physiochemical properties of TCP are listed in Table 1.

High-silica zeolite powders of FAU framework were provided by suppliers. The names, suppliers and Si/Al ratios of zeolites are listed in Table 2.

2.2. Adsorption experiments

Batch adsorption experiments were conducted in demineralized water. The FAU zeolites (30 mg L^{-1}) were dosed in the 100 ml TCP aqueous solution with the TCP concentrations ranging from 0 to 50 μmol L^{-1}. After the equilibrium time of 24 h at room temperature (25 ± 1 °C), the zeolites were separated from the TCP solution by membrane filtration (0.2 μm syringe filter, Whatman SPARTAN™). This equilibrium time is expected to be sufficient, as shown by Zhang et al. [24], who measured the adsorption of TCP on FAU30.

2.3. High performance liquid chromatography (HPLC) analyses

The concentration of filtrated TCP solution was determined by HPLC (Shimadzu, Japan) with a C18 column (Phenomenex® KINETEX, 4.6 mm) at 30 °C. HPLC-grade acetonitrile (Sigma-Aldrich, the Netherlands) and ultra-pure water (Milli-Q ultra-pure water system) were mixed as the mobile phase with a ratio of 65:35 (v:v). The flow rate of the mobile phase was 1.0 ml min^{-1}. The wavelength of the UV detector was set at 280 nm.

2.4. Monte Carlo simulation

2.4.1. Force fields

The force field parameters for TCP, water and zeolites were taken from the Generalized Amber Force Field (GAFF) [61], Extended Single Point Charge (SPC/E) [62] and Clay Force Field (ClayFF) [63] models, respectively. The choice of these force fields is based on the study by Narasimhan et al. [64] in which it was shown that a similar force field combination was able to reproduce experimental results of the adsorption of paracresol and water onto MFI zeolites reasonably well. As discussed earlier, the adsorption isotherms computed from MC simulations were used only to obtain physical insight into the adsorption mechanisms. To this end, no modifications in the force fields or cross interactions parameters between the different species were applied to achieve better agreement with the experimental measurements. Moreover, exhaustive simulations using various other force field combinations was also not the scope of this study. All the force field parameters used in this study are listed in Table S1 in the Supporting Information.

Table 2
Information of the high-silica zeolites studied.

Zeolite name[a]	Product name	Supplier	Si/Al ratio[b]
FAU250	390HUA	Tosoh	250
FAU50	385HUA	Tosoh	50
FAU40	CBV901	Zeolyst	40
FAU30	CBV760	Zeolyst	30

[a] The names of the zeolites in this study were based on the framework type and the Si/Al ratio.
[b] Si/Al ratio provided by the suppliers.

2.4.2. Simulation details

All MC simulations were carried out using the Cassandra open source software package V1.2 [65]. In the Cassandra software package the chemical potential, which is imposed in the GCMC simulations is shifted with a value containing the partition functions of the molecules which are inserted in the simulation box. To be able to convert this shifted chemical potential to equilibrium concentration additional simulations are performed. The details of the applied method is shown in Section S2 in the Supporting Information.

Short-range van der Waals interactions were considered by the (12–6) Lennard-Jones potential (see Equation S1 in the Supporting Information). For the mixed pair potentials the Lorentz-Berthelot mixing rules [66] were used (see Equation S2 in the Supporting Information). Long-range electrostatic interactions were considered by the Ewald summation method [67] with a relative precision of 10^{-5}. For the LJ and electrostatic interactions a cutoff radius of 14 Å with analytic tail correction was applied. In all simulations, 8 unit cells per simulation box (a 2x2x2 supercell) were used and periodic boundary conditions were imposed in all direction. The zeolite framework was considered rigid in all simulations. This approach is often being applied in simulations of nanoporous materials to prevent the necessity of excessive computational efforts [68]. Zeolite frameworks with specified Si/Al ratios were created based on the structures reported by Hriljac et al. [69]. The desired Si/Al ratios were achieved by randomly exchanging silicon atoms with aluminum atoms while obeying Löwnstein's rule which states that the Al – O – Al bonds are prohibited in

Table 1
The physicochemical characteristics of TCP.

IUPAC name	Chemical formula	Molecular weight (g mol^{-1})	Solubility in water (mg L^{-1}) [a]	Log D at pH 6 [b]	pka [b]	Chemical structure
2,4,6-trichlorophenol	$C_6H_3Cl_3O$	197.45	800	3.58	6.2 ± 0.4	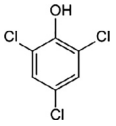

[c]Estimated by Hyperchem 7.0 after geometric optimization.
[a] Estimated by EPIWEB 4.1.
[b] Estimated by ACD/LABs PhysChem Module (Algorithm Version: 5.0.0.184).

zeolites [69]. The number of sodium atoms were adjusted in accordance to the number of aluminum atoms to ensure the electro-neutrality of the framework. The sodium atoms were fixed at their crystallographic position in order to simplify the simulation scheme. It is important to note that the choice of fixing the sodium or allowing it to move in the zeolite framework may vastly affect the computed adsorption isotherms as shown by Calero et al. [70] in alkane adsorption onto FAU zeolites. The effect of fixing the sodium ion to the framework has not yet been studied in MC simulations of adsorption from the liquid phase. Thus, further investigation is needed to show the exact magnitude of this effect on the computed adsorption isotherms.

To obtain the adsorption isotherms, Configurational-Bias Monte Carlo (CBMC) simulations in the grand-canonical (μVT) ensemble (GCMC) were performed [67]. The following types of trial moves were used: translations (~12%), rotations (~12%), partial regrowth (~10%) and molecule exchanges with the reservoir (~66%). In all MC runs an equilibration period of 5,000,000 MC steps was performed. After the equilibration, production runs of 15,000,000 MC steps were carried out, from which ensemble averages were calculated.

The MC simulations were performed for the FAU250, FAU50, FAU40 and FAU30 frameworks. The Si/Al ratios and the number of Al atoms in the framework are listed in Table 3. The simulated zeolite frameworks cover a wider Si/Al range compared to the batch experiments. The Si/Al in simulations was in the range 5 – 250, while in experiments was in the range 30 – 250.

3. Results and discussion

3.1. TCP adsorption on FAU zeolite

The experimental results of TCP adsorption isotherms on FAU zeolites with varying Al content are shown in Fig. 3. The adsorption isotherms of TCP on FAU250, FAU50 and FAU40 had an S shape, while the adsorption isotherm of FAU30 did not reach a plateau in the experimental concentration range. It is assumed that the observed adsorption isotherm was the beginning stage of S-shaped isotherm and the maximum adsorption loading of TCP on FAU30 will be achieved with the increase of TCP equilibrium concentration. As observed from the adsorption plateaus of S-shaped isotherms, the maximum adsorption loading of TCP on FAU250, FAU50 and FAU40 followed the order FAU250 > FAU50 > FAU40. This indicates that TCP adsorption on FAU zeolites, including the TCP loading and the shape of the adsorption isotherms, was driven by the Si/Al ratio of the zeolite. In the studied equilibrium concentration range of 0 – 20 μmol L^{-1} the highest TCP adsorption loading on FAU30 was < 400 μmol g^{-1}.

In Fig. 4, the simulated adsorption isotherms of TCP on FAU zeolites with varying Al contents are shown. As shown in Fig. 4, the simulated adsorption isotherms of all five FAU zeolites, including FAU5 (which was not tested in batch experiments), were S-shaped. The adsorption loadings of TCP on FAU zeolites followed the same order as in the experiments: FAU250 > FAU50 > FAU40 > FAU30 > FAU5. As can be seen in Fig. 4, the adsorption isotherms for FAU250 and FAU50 computed from MC simulations exhibited almost identical maximum loading to the respective experimentally measured isotherms. By

Table 3
The list of the FAU zeolite frameworks used in the MC simulations.

Zeolite name	Si/Al ratio in simulated box	Numbers of Al atom in the framework	Number of Supercages/ Sodalite cages in the framework
FAU250	255	6	64/64
FAU50	50	30	
FAU40	41	37	
FAU30	30	50	
FAU5	9	156	

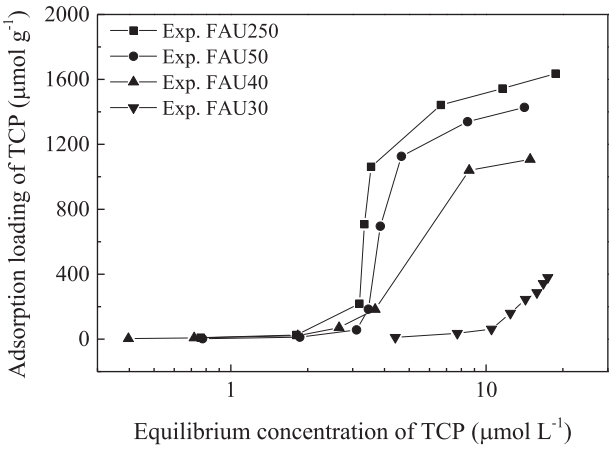

Fig. 3. The adsorption isotherm of TCP on FAU zeolites from batch experiments represented by solid symbols.

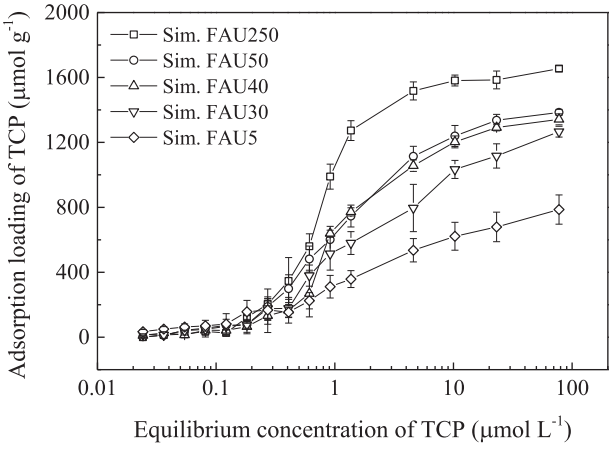

Fig. 4. The adsorption isotherm of TCP on FAU zeolites from MC simulation represented by open symbols.

incorporating more Al atoms in the framework, the S-shape of the adsorption isotherms became less pronounced. This is also in line with the experimental measurements shown in Fig. 3, indicating that MC simulations captures the effect of Si/Al ratio on the shape of the adsorption isotherm.

The adsorption loading of TCP on FAU40 was underestimated in the simulation, showing a deviation of ~ 300 mg g^{-1} from experimental results. The simulated adsorption isotherms of FAU30 zeolites was S-shaped with a maximum TCP loading of ~1200 mg g^{-1} (Fig. 4), while the adsorption loading of FAU30 obtained from experiments was ~400 mg g^{-1}, which is observed from an C-shaped isotherm without adsorption plateau (Fig. 3). The equilibrium concentration at which the adsorption step occurs in the isotherms computed from MC simulations is not as pronounced as in the experimentally measured ones, and moreover, it seems to deviate quite significantly.

The possible reason for the discrepancies between experiments and MC simulations is the force fields representing the adsorbent and adsorbates, as well as the fact that sodium ions are fixed in the FAU crystal. Since there were no prior MC simulations of the co-adsorption of water and TCP onto zeolites, the force fields representing water, TCP and zeolites were chosen based on the study by Narasimhan et al. [64], where the adsorption of water and paracresol onto MFI zeolites was studied. As stated earlier, no modification or refitting of the individual force fields was performed in the current study. However, such modifications in order to improve the accuracy of the simulations, can be realized in several ways: e.g. by optimizing the Lennard-Jones parameters or atomic charges, by explicitly including polarization effects,

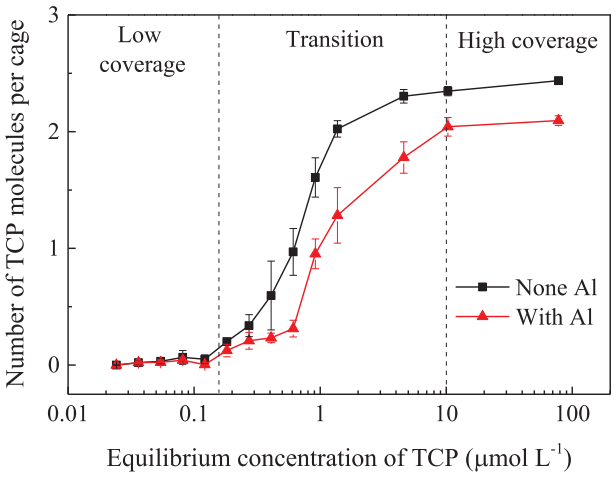

Fig. 5. The number of adsorbed TCP molecules in the supercages of FAU250 zeolite computed from the MC simulations.

and by modifying the intermolecular interactions between Al atoms and the adsorbates. Although such modifications may give a better agreement between the simulation and experimental results, their implementation requires significant computational effort which is out of the scope of this study.

3.2. The adsorption mechanisms behind the S-shaped adsorption isotherms

Since the adsorption isotherms for FAU250 computed from MC simulations exhibited almost identical maximum loading to the experimentally measured adsorption isotherms, the MC simulation results of FAU250 were further used to understand the adsorption mechanisms of S-shaped adsorption isotherm.

In Fig. 5, the average number of adsorbed TCP molecules in the supercages of FAU250 are plotted as a function of the equilibrium concentration of TCP. The number of adsorbed TCP molecules increased with the increase of TCP equilibrium concentration and the S-shaped curves is observed from Fig. 5. The S-shaped curves were qualitatively characterized by a division of three stages. At the low coverage range (equilibrium concentration < 0.15 μmol L^{-1}), a minimal amount of TCP molecules (close to 0) were adsorbed on the FAU250 zeolites. There was 0 to 1 TCP molecule adsorbed in the supercages. The average number of adsorbed TCPs increased considerably at the transition stage (equilibrium concentration of 0.15 to 10 μmol L^{-1}). At the stage of high coverage (equilibrium concentration > 10 μmol L^{-1}), the maximum number of adsorbed TCP is observed from the plateau.

As shown in Fig. 5, the S-shaped curves are observed for both supercages without Al and supercages with Al, while the maximum number of adsorbed TCP in two types of supercages varied. A supercage provided accommodation to approximately 2 TCP molecules in Al containing cages and 2.5 TCP molecules in the none-Al containing cage, respectively. In the supercages with no Al atom, a maximum of 3 TCP molecules could be adsorbed.

The simulated arrangement of the adsorbed TCP molecules with water molecules in the supercages without Al are shown in Fig. 6. When 1 TCP molecule was adsorbed in the supercage, TCP preferably excluded the water molecules in between and was arranged close to the wall of the cage (Fig. 6a). In the supercages with 2 or 3 adsorbed TCP molecules, less water molecules were adsorbed and the TCP molecules obtained a parallel configuration, with benzene rings facing each other (Fig. 6b and 6c).

To obtain further information about the structure of adsorbed molecules in the framework, the radial distribution function (RDF) was calculated [66]. The RDF, usually represented as g(r), defines the probability of finding a particle at distance r from another tagged particle. In Fig. 7, the RDF between the center of mass of benzene rings on the FAU250 framework at TCP equilibrium concentration of 77.6 μmol L^{-1} is shown. From Fig. 7, it is observed that the characteristic distance between two TCP molecules was ~3.7 Å, which is a typical packing distance between π - π stacked aromatic groups (3.4 Å − 3.8 Å). This is in line with literature [71,72] as TCP molecules in aqueous solutions could experience π – π interactions, as a form of lateral interactions in the supercages. The lateral interaction considerably promoted TCP adsorption at the transition stage (Fig. 5), and led to the S-shaped adsorption isotherm. This finding is in line with the work of Walton et al. [73]. who attributed the steps in the adsorption isotherms for CO_2 on metal–organic frameworks to the sudden clustering of CO_2 molecules in the pores.

The π- π interaction could occur between two TCP molecules with C – C π electrons, originating from benzene rings of TCP molecules. The C – C π electrons of TCP molecules could shift from the center of the benzene ring due to electron donating of hydroxyl groups and electron withdrawing of chlorine atoms to the conjugated π electron. Thus, two TCP molecules could form a π - π interaction with an offset stacked conformation other than a perfect face-to-face alignment, as clearly shown from the simulation snapshots in Fig. 6. In this conformation, most of the surface of TCP molecules were covered by each other and the π - π interaction between TCP molecules is expected to be strong [74]. Although there is no explicit term to account for the π- π interactions in the force fields used, the use of fixed-point charges can reproduce these interactions [75,76] as shown by the characteristic distances and orientation of the TCP molecules in Figs. 6 and 7.

3.3. The effect of water adsorption on the occurrence of S-shaped adsorption isotherms and TCP adsorption

In Fig. 8, the number of adsorbed water molecules in supercages of FAU250 is plotted as a function of the equilibrium concentration of TCP. Fig. 8 shows that the number of water molecules in the supercages of FAU250 decreased with equilibrium concentration of TCP. Al-containing cages had a higher number of adsorbed water molecules than the cages without Al. At the higher equilibrium concentration (> 77 μmol L^{-1}), about 8 water molecules per cage were adsorbed in the supercages with Al atom, while approximately 5 molecules per cage were adsorbed in the supercages without Al atom. Compared to water adsorption in sodalite cages (0 – 3 water molecules per cage, Fig. 10), more water molecules were adsorbed in supercages (8 – 25 water molecules per cage, Fig. 8). This can be attributed to the much less space inside sodalite cages than supercages [56].

The arrangement of the adsorbed water and TCP molecules in the Al-containing supercages are shown in Fig. 9. The distance between hydrogen atoms from water and the oxygen atoms of zeolites, which are connected to Al atom, was computed to be 1.7 Å. In the Al-containing supercages with one TCP molecule adsorbed, a total number of 19 water molecules were adsorbed (Fig. 9a), while 10 water molecules were adsorbed in the supercages with 2 adsorbed TCP molecules (Fig. 9b). In the none Al-containing supercages, however, 14 water molecules were co-adsorbed along with one TCP molecule, and 3 water molecules were co-adsorbed along with two TCP molecules (Fig. 6). This is in line with the results presented in Fig. 9, where it is shown that more water molecules were adsorbed in the supercages with Al. The Al-containing supercages with 3 adsorbed TCP molecules were not found in the simulation box, since water molecules hinder the TCP adsorption due to the limited space in the supercages.

The number of adsorbed water molecules in sodalite cages of FAU250 zeolites is plotted as a function of the equilibrium concentration of TCP in Fig. 10. As shown in Fig. 10, water adsorption in sodalite cages was not affected by the equilibrium concentration of TCP. The sodalite cages with Al atom had an average number of approximately 1.5 water molecules per cage with a variation from 1 to 2 water molecules per cage, while the sodalite cages without Al atom exhibited

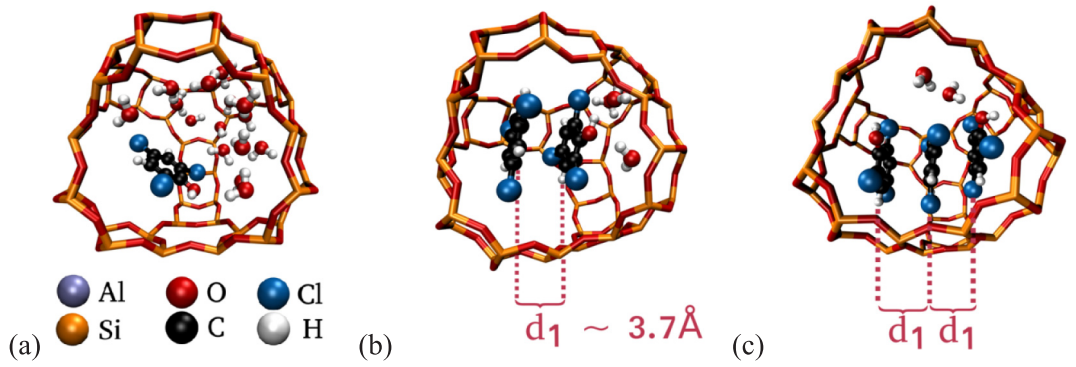

Fig. 6. The arrangements of TCP and water molecules in the none-Al containing supercages of FAU250 zeolites: (a) 1 TCP, (b) 2 TCP, (c) 3 TCP molecule(s) per cage at TCP equilibrium concentration equal to (a) 4.6, (b) 77.6 and (c) 77.6 μmol L^{-1}. The characteristic distance between the center of mass of the benzene rings in the TCP molecules is shown as d_1.

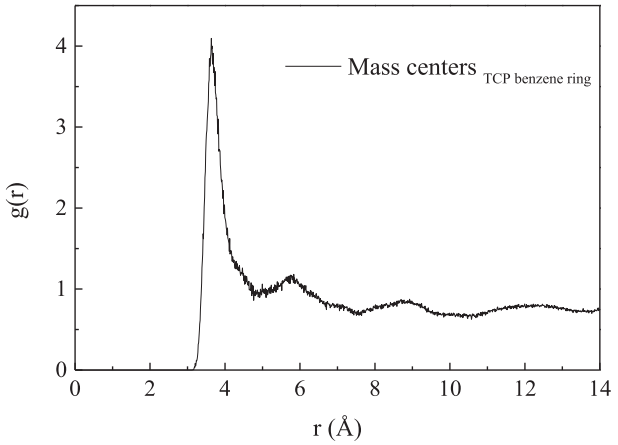

Fig. 7. Radial distribution function (RDF) of mass center of benzene rings in TCP molecules adsorbed on FAU250 at a TCP equilibrium concentration equal to 77.6 μmol L^{-1}. The characteristic distance between two benzene rings is indicated by the first peak of the RDF around r = 3.7 Å.

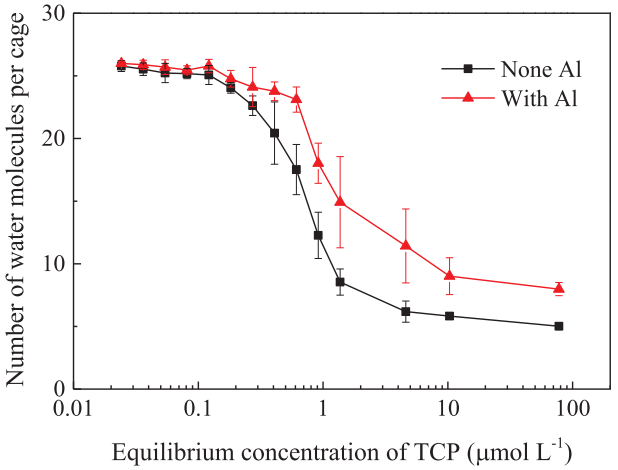

Fig. 8. Number of adsorbed water molecules in the supercages of FAU250 zeolite.

almost no ability for water adsorption.

The RDF between the hydrogen atom from water and the oxygen atom connected to Al atom of FAU250 zeolites was calculated to determine the structures of adsorbed water molecules on FAU250 zeolite. As shown in Fig. 11a, one peak is observed at the distance of 1.7 Å, which is the typical H-bond length [77]. Thus, we can safely conclude

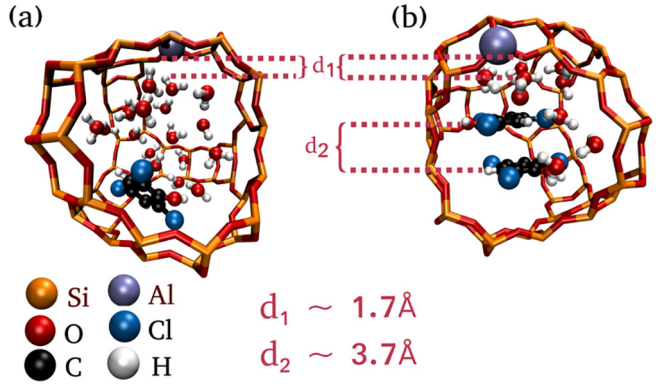

Fig. 9. The arrangements of TCP and water molecules in the supercages of FAU250 zeolite with Al atom: (a) 1 TCP molecule per cage at the equilibrium concentration equal to 4.6 μmol L^{-1} (b) 2 TCP molecules per cage at the equilibrium concentration equal to 77.6 μmol L^{-1}.

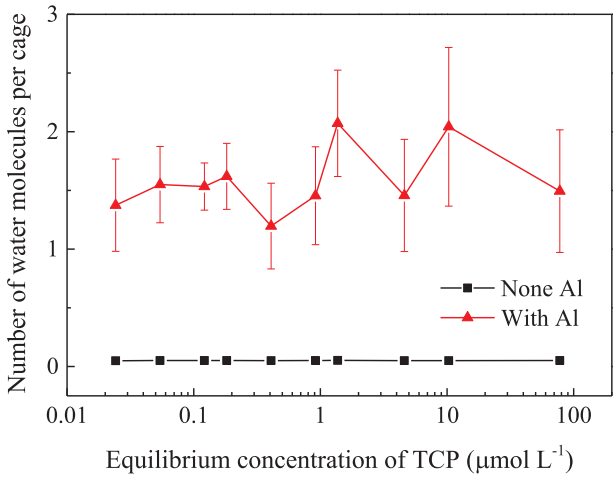

Fig. 10. Number of adsorbed water molecules in the sodalite cages of FAU250 zeolite.

that water molecules were being adsorbed on FAU zeolites by forming H-bonds with the framework. Narasimhan et al. [60] indicated that the existence of water clusters could weaken the interaction of water molecules with zeolites, as well as the interaction of OMPs with zeolites, which, however, would strengthen the interactions between OMPs and water. The two wide peaks at distances of 2.9 Å and 4.0 Å shown in Fig. 11a, indicate that water molecules which do not form H-bonds with the FAU framework formed water clusters.

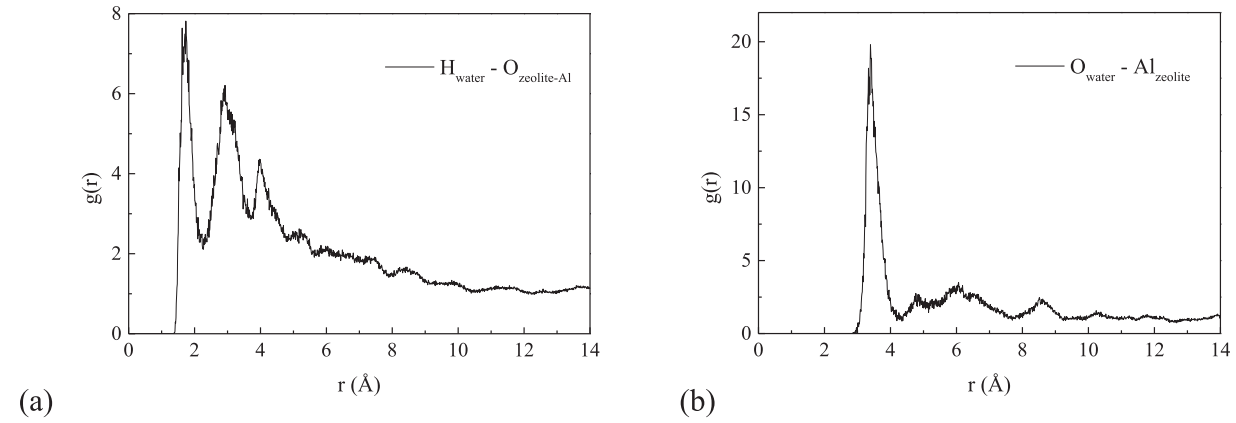

Fig. 11. Radial distribution function (RDF) of (a) H atom from water molecules and O atom connected to Al atom of FAU250 framework; (b) O atom from water molecules and Al atom from FAU250 framework at TCP equilibrium concentration equal to 77.6 μmol L^{-1}.

As shown in Fig. 11b, the RDF between the O atom of adsorbed water molecules and Al atom of zeolite framework has a strong peak at distance of approximately 3.4 Å. Bolis et al. [78] suggested that water molecules were adsorbed on zeolites by interacting with the –Si-O-Si- groups of zeolites. The distance of 3.4 Å between Al atom of zeolites and water molecules, shown in Fig. 11b, clearly indicate that there was an additional driving force for water adsorption on the supercages (Fig. 8) and sodalite cages (Fig. 10) of the FAU zeolite. The additional driving forces from Al atoms might cause an extra number of water molecules to be adsorbed in the supercages (Fig. 8) and sodalite cages (Fig. 10). Due to the additional water adsorption on Al atom, FAU zeolite with higher Al content (lower Si/Al ratio) had a lower TCP adsorption loading and less pronounced S-shaped adsorption isotherms (Figs. 3 and 4). Zhang et al. [24] studied TCP adsorption on FAU zeolites with Si/Al ratio 30 and observed no plateau from the adsorption isotherm, which confirms the finding in the present study.

The supercages of FAU zeolite with large pore opening and inner sizes provided the basic conditions for the accommodation of multiple TCP molecules and their lateral interaction in the presence of water molecules, which was crucial for the occurrence of the S-shaped adsorption isotherms. In the zeolite frameworks with channels, the adsorbed OMPs preferred to be located in the channels and channel intersections, whereas water molecules preferably adsorbed in the vicinity of the OMP molecules [59,79,80]. Due to the hindering of water molecules, the lateral interaction of adsorbed OMP molecules would be negligible. Therefore, the S-shaped adsorption isotherm was not observed in previous literature, which studied OMP adsorption on zeolites frameworks with channels, e.g. BEA and MFI type zeolites [81–83].

4. Conclusions

In this study, MC simulations were used to explain the mechanism of S-shaped adsorption isotherms of TCP adsorption on high-silica FAU zeolites. This study shows that the occurrence of S-shaped adsorption isotherms was attributed to the lateral interaction of TCP, e.g., the π- π interaction. The supercages of FAU zeolites provided a possible accommodation for multiple TCP molecules as a potential condition of lateral interactions of TCP. Water molecules were adsorbed in the sodalite cages and supercages of FAU zeolites by forming H-bonds with the framework of zeolites. Compared to the none Al-containing supercages, more water molecules were stably adsorbed as water clusters in the supercages of FAU zeolites with Al content. An additional amount of adsorbed water molecules in Al-containing supercages could inhibit TCP adsorption and could prevent the occurrence of an S-shaped adsorption isotherm. FAU zeolites with higher Si/Al ratio, therefore, had evident S-shaped adsorption isotherms, and, meanwhile, achieved higher TCP adsorption loadings compared to FAU zeolites with lower Si/Al ratios. MC simulation has thus been proven to be a powerful tool to study the adsorption of OMPs in water to support experimental results. Performing MC simulation will further allow investigating the adsorption mechanisms of OMP adsorption from the view of molecular interaction between OMPs, OMP and adsorbents as well as water and adsorbents.

The unfavourable adsorption of OMPs have been widely observed from OMP adsorption on solid adsorbents. The low adsorption capacity would be followed by a steep increase of OMP adsorption capacity at a certain equilibrium concentration, showing the typical feature of S-shaped isotherms. This study suggests that the increase of OMP adsorption capacity was caused by the interaction between OMPs. Except for the π- π interaction between TCP molecules in this study, various types of OMP interactions might exist as driving forces for OMP adsorption, since the physicochemical properties of OMPs also vary.

Acknowledgements

This work was sponsored by NWO Exacte Wetenschappen (Physical Sciences) for the use of supercomputer facilities, with financial support from the Nederlandse Organisatie voor Wetenschappelijk Onderzoek (Netherlands Organization for Scientific Research, NWO). T.J.H.V. acknowledges NWO-CW (Chemical Sciences) for a VICI grant. The experimental work was financed by the Supplement for Top Consortia for Knowledge and Innovation (TKIs) of the Ministry of Economic Affairs. Nan Jiang acknowledges the China Scholarship Council for her PhD scholarship under the State Scholarship Fund (No.201406120042).

Appendix A. Supplementary data

Supplementary data to this article can be found online at https://doi.org/10.1016/j.cej.2019.123968.

References

[1] T. Ennaert, J. Van Aelst, J. Dijkmans, R. De Clercq, W. Schutyser, M. Dusselier, D. Verboekend, B.F. Sels, Potential and challenges of zeolite chemistry in the catalytic conversion of biomass, Chem. Soc. Rev. 45 (2016) 584–611.
[2] A. Alonso, J. Moral-Vico, A.A. Markeb, M. Busquets-Fite, D. Komilis, V. Puntes, A. Sanchez, X. Font, Critical review of existing nanomaterial adsorbents to capture carbon dioxide and methane, Sci. Total Environ. 595 (2017) 51–62.
[3] L. Zhang, Y. Peng, J. Zhang, L. Chen, X. Meng, F.-S. Xiao, Adsorptive and catalytic properties in the removal of volatile organic compounds over zeolite-based materials, Chinese J Catal 37 (2016) 800–809.
[4] Y. Li, L. Li, J. Yu, Applications of zeolites in sustainable chemistry, Chem 3 (2017) 928–949.
[5] S. Wang, Y. Peng, Natural zeolites as effective adsorbents in water and wastewater treatment, Chem. Eng. J. 156 (2010) 11–24.
[6] S. Mohan, P. Dinesha, S. Kumar, NOx reduction behaviour in copper zeolite

catalysts for ammonia SCR systems: A review, Chem. Eng. J. 123253 (2019).
[7] A. Burton, Recent trends in the synthesis of high-silica zeolites, Cat. Rev. 60 (2018) 132–175.
[8] P. Jacobs, E.M. Flanigen, J. Jansen, H. van Bekkum, Introduction to zeolite science and practice, Elsevier, 2001.
[9] T. Maesen, B. Marcus, The zeolite scene - an overview, in: Studies in Surface Science and Catalysis, Elsevier 2001, pp. 1-9.
[10] R.F. Lobo, High-silica zeolites: From synthesis to structure, Abstr. Pap. Am. Chem. Soc. 213 (1997) 345-COLL.
[11] T. Maesen, The zeolite scene - an overview, in: J. Cejka, H.V. Bekkum, A. Corma, F. Schuth (Eds.) Introduction to Zeolite Science and Practice, Elsevier Science BV Amsterdam 2007, pp. 1-12.
[12] G.V. Tsitsishvili, Physicochemical properties of high silica L and clinoptilolite zeolites, in: Molecular Sieves, American Chemical Society 1973, pp. 291-298.
[13] C. Baerlocher, L.B. McCusker, Database of zeolite structures, in, 2017.
[14] N. Jiang, R. Shang, S.G. Heijman, L.C. Rietveld, High-silica zeolites for adsorption of organic micro-pollutants in water treatment: A review, Water Res (2018).
[15] A. Rossner, S.A. Snyder, D.R.U. Knappe, Removal of emerging contaminants of concern by alternative adsorbents, Water Res. 43 (2009) 3787–3796.
[16] I. Braschi, S. Blasioli, L. Gigli, C.E. Gessa, A. Alberti, A. Martucci, Removal of sulfonamide antibiotics from water: Evidence of adsorption into an organophilic zeolite Y by its structural modifications, J. Hazard. Mater. 178 (2010) 218–225.
[17] D.J. de Ridder, J.Q.J.C. Verberk, S.G.J. Heijman, G.L. Amy, J.C. van Dijk, Zeolites for nitrosamine and pharmaceutical removal from demineralised and surface water: Mechanisms and efficacy, Sep. Purif. Technol. 89 (2012) 71–77.
[18] N.A.S. Amin, J. Akhtar, H.K. Rai, Screening of combined zeolite-ozone system for phenol and COD removal, Chem. Eng. J. 158 (2010) 520–527.
[19] C.H. Giles, D. Smith, A. Huitson, A general treatment and classification of the solute adsorption isotherm, I. Theoretical, J Colloid Interf Sci 47 (1974) 755–765.
[20] G. Limousin, J.P. Gaudet, L. Charlet, S. Szenknect, V. Barthès, M. Krimissa, Sorption isotherms: A review on physical bases, modeling and measurement, Appl. Geochem. 22 (2007) 249–275.
[21] V.J. Inglezakis, S.G. Poulopoulos, H. Kazemian, Insights into the S-shaped sorption isotherms and their dimensionless forms, Micropor. Mesopor. Mat. 272 (2018) 166–176.
[22] C. Hinz, Description of sorption data with isotherm equations, Geoderma 99 (2001) 225–243.
[23] V. Simon, A. Thuret, L. Candy, S. Bassil, S. Duthen, C. Raynaud, A. Masseron, Recovery of hydroxycinnamic acids from renewable resources by adsorption on zeolites, Chem. Eng. J. 280 (2015) 748–754.
[24] Y. Zhang, R.G. Mancke, M. Sabelfeld, S.-U. Geissen, Adsorption of trichlorophenol on zeolite and adsorbent regeneration with ozone, J. Hazard. Mater. 271 (2014) 178–184.
[25] D.L. Sparks, 5 - Sorption phenomena on soils, in: D.L. Sparks (Ed.), Environmental Soil Chemistry (Second, Edition), Academic Press Burlington, 2003, pp. 133–186.
[26] A.D. Mackie, B. Tavitian, A. Boutin, A.H. Fuchs, Vapour-liquid phase equilibria predictions of methane–alkane mixtures by Monte Carlo simulation, Mol. Simulat. 19 (1997) 1–15.
[27] C.E. Wilmer, M. Leaf, C.Y. Lee, O.K. Farha, B.G. Hauser, J.T. Hupp, R.Q. Snurr, Large-scale screening of hypothetical metal–organic frameworks, Nat. Chem. 4 (2012) 83.
[28] D. Bahamon, A. Díaz-Márquez, P. Gamallo, L.F. Vega, Energetic evaluation of swing adsorption processes for CO2 capture in selected MOFs and zeolites: Effect of impurities, Chem. Eng. J. 342 (2018) 458–473.
[29] R.B. Getman, Y.-S. Bae, C.E. Wilmer, R.Q. Snurr, Review and analysis of molecular simulations of methane, hydrogen, and acetylene storage in metal–organic frameworks, Chem. Rev. 112 (2011) 703–723.
[30] M.t. Erdos, M.F. de Lange, F. Kapteijn, O.A. Moultos, T.J. Vlugt, In silico screening of metal–organic frameworks for adsorption-driven heat pumps and chillers, ACS Appl. Mater. Interfaces 10 (2018) 27074-27087.
[31] S. Kayal, A. Chakraborty, Activated carbon (type Maxsorb-III) and MIL-101 (Cr) metal organic framework based composite adsorbent for higher CH4 storage and CO2 capture, Chem. Eng. J. 334 (2018) 780–788.
[32] B. Smit, a. Krishna, Molecular simulations in zeolitic process design, Chem. Eng. Sci. 58 (2003) 557-568.
[33] A.H. Fuchs, A.K. Cheetham, Adsorption of guest molecules in zeolitic materials: computational aspects, ACS Publications (2001).
[34] S. Dang, L. Zhao, Q. Yang, M. Zheng, J. Zhang, J. Gao, C. Xu, Competitive adsorption mechanism of thiophene with benzene in FAU zeolite: The role of displacement, Chem. Eng. J. 328 (2017) 172–185.
[35] P. Cosoli, M. Ferrone, S. Pricl, M. Fermeglia, Hydrogen sulphide removal from biogas by zeolite adsorption Part I. GCMC molecular simulations, Chem. Eng. J. 145 (2008) 86–92.
[36] E.A. Müller, L.F. Rull, L.F. Vega, K.E. Gubbins, Adsorption of water on activated carbons: a molecular simulation study, J. Phys. Chem. 100 (1996) 1189–1196.
[37] K.R. Matranga, A.L. Myers, E.D. Glandt, Storage of natural gas by adsorption on activated carbon, Chem. Eng. Sci. 47 (1992) 1569–1579.
[38] A.F. Dalebrook, W. Gan, M. Grasemann, S. Moret, G. Laurenczy, Hydrogen storage: beyond conventional methods, Chem. Commun. 49 (2013) 8735–8751.
[39] L.-C. Lin, A.H. Berger, R.L. Martin, J. Kim, J.A. Swisher, K. Jariwala, C.H. Rycroft, A.S. Bhown, M.W. Deem, M. Haranczyk, In silico screening of carbon-capture materials, Nat. Mater. 11 (2012) 633.
[40] J. Jänchen, D. Ackermann, H. Stach, W. Brösicke, Studies of the water adsorption on zeolites and modified mesoporous materials for seasonal storage of solar heat, Solar Energy 76 (2004) 339–344.
[41] T.C. Bowen, R.D. Noble, J.L. Falconer, Fundamentals and applications of pervaporation through zeolite membranes, J. Membr. Sci. 245 (2004) 1–33.
[42] T. Tomita, K. Nakayama, H. Sakai, Gas separation characteristics of DDR type zeolite membrane, Micropor. Mesopor. Mat. 68 (2004) 71–75.
[43] S. Babel, T.A. Kurniawan, Low-cost adsorbents for heavy metals uptake from contaminated water: a review, J. Hazard. Mater. 97 (2003) 219–243.
[44] A. Metes, D. Kovacevic, D. Vujevic, S. Papic, The role of zeolites in wastewater treatment of printing inks, Water Res. 38 (2004) 3373–3381.
[45] Z. Du, G. Manos, T.J. Vlugt, B. Smit, Molecular simulation of adsorption of short linear alkanes and their mixtures in silicalite, AlChE J. 44 (1998) 1756–1764.
[46] E.J. Maginn, A.T. Bell, D.N. Theodorou, Sorption thermodynamics, siting, and conformation of long n-alkanes in silicalite as predicted by configurational-bias Monte Carlo integration, J. Phys. Chem. 99 (1995) 2057–2079.
[47] B. Smit, J.I. Siepmann, Computer simulations of the energetics and siting of n-alkanes in zeolites, J. Phys. Chem. 98 (1994) 8442–8452.
[48] S. Calero, P. Gómez-Álvarez, On the performance of FAU and MFI zeolites for the adsorptive removal of a series of volatile organic compounds from air using molecular simulation, Phys. Chem. Chem. Phys. 17 (2015) 26451–26455.
[49] C.C. Brunchi, J.M. Castillo Sanchez, A.I. Stankiewicz, H.J. Kramer, T.J. Vlugt, Adsorption of volatile organic compounds. Experimental and theoretical study, Ind. Eng. Chem. Res. 51 (2012) 16697–16708.
[50] J. Gao, L. Liu, X. Liu, H. Zhou, S. Huang, Z. Wang, Levels and spatial distribution of chlorophenols–2, 4-dichlorophenol, 2, 4, 6-trichlorophenol, and pentachlorophenol in surface water of China, Chemosphere 71 (2008) 1181–1187.
[51] K. Verschueren, Handbook of environmental data on organic chemicals Vol. 1 John Wiley and Sons Inc, 2001.
[52] B.H. Hameed, I.A.W. Tan, A.L. Ahmad, Adsorption isotherm, kinetic modeling and mechanism of 2,4,6-trichlorophenol on coconut husk-based activated carbon, Chem. Eng. J. 144 (2008) 235–244.
[53] A.H. Yonli, I. Batonneau-Gener, J. Koulidiati, Adsorptive removal of alpha-endosulfan from water by hydrophobic zeolites. An isothermal study, J. Hazard. Mater. 203 (2012) 357–362.
[54] B. Koubaissy, G. Joly, I. Batonneau-Gener, P. Magnoux, Adsorptive removal of aromatic compounds present in wastewater by using dealuminated faujasite zeolite, Ind. Eng. Chem. Res. 50 (2011) 5705–5713.
[55] S. Fukahori, T. Fujiwara, R. Ito, N. Funamizu, pH-Dependent adsorption of sulfa drugs on high silica zeolite: Modeling and kinetic study, Desalination 275 (2011) 237–242.
[56] C. Baerlocher, L.B. McCusker, D.H. Olson, Atlas of zeolite framework types, Elsevier, 2007.
[57] D. Faux, W. Smith, T. Forester, Molecular dynamics studies of hydrated and dehydrated Na^+-zeolite-4A, J. Phys. Chem. B 101 (1997) 1762–1768.
[58] A.O. Yazaydin, Molecular simulation of the adsorption of organics from water, in: Worcester Polytechnic Institute Worcester, MA, 2007.
[59] R.F. DeJaco, P. Bai, M. Tsapatsis, J.I. Siepmann, Adsorptive separation of 1-Butanol from aqueous solutions using MFI- and FER-type zeolite frameworks: A Monte Carlo study, Langmuir 32 (2016) 2093–2101.
[60] L. Narasimhan, B. Kuchta, O. Schaef, P. Brunet, P. Boulet, Mechanism of adsorption of p-cresol uremic toxin into faujasite zeolites in presence of water and sodium cations – A Monte Carlo study, Micropor. Mesopor. Mat. 173 (2013) 70–77.
[61] J. Wang, R.M. Wolf, J.W. Caldwell, P.A. Kollman, D.A. Case, Development and testing of a general amber force field, J. Comput. Chem. 25 (2004) 1157–1174.
[62] H.J.C. Berendsen, J.R. Grigera, T.P. Straatsma, The missing term in effective pair potentials, J. Phys. Chem. 91 (1987) 6269–6271.
[63] R.T. Cygan, J.-J. Liang, A.G. Kalinichev, Molecular models of hydroxide, oxyhydroxide, and clay phases and the development of a general force field, J. Phys. Chem. B 108 (2004) 1255–1266.
[64] L. Narasimhan, P. Boulet, B. Kuchta, O. Schaef, R. Denoyel, P. Brunet, Molecular simulations of water and paracresol in MFI zeolite-a Monte Carlo study, Langmuir 25 (2009) 11598–11607.
[65] J.K. Shah, E. Marin-Rimoldi, R.G. Mullen, B.P. Keene, S. Khan, A.S. Paluch, N. Rai, L.L. Romanielo, T.W. Rosch, B. Yoo, Cassandra: An open source Monte Carlo package for molecular simulation, J. Comput. Chem. 38 (2017) 1727–1739.
[66] M.P. Allen, D.J. Tildesley, Computer simulation of liquids, Oxford University Press, 2017.
[67] D. Frenkel, B. Smit, Understanding molecular simulation: from algorithms to applications, Elsevier, 2001.
[68] T.J. Vlugt, M. Schenk, Influence of framework flexibility on the adsorption properties of hydrocarbons in the zeolite silicalite, J. Phys. Chem. B 106 (2002) 12757–12763.
[69] J. Hriljac, M. Eddy, A. Cheetham, J. Donohue, G. Ray, Powder neutron diffraction and 29Si MAS NMR studies of siliceous zeolite-Y, J. Solid State Chem. 106 (1993) 66–72.
[70] S. Calero, D. Dubbeldam, R. Krishna, B. Smit, T.J.H. Vlugt, J.F.M. Denayer, J.A. Martens, T.L.M. Maesen, Understanding the role of sodium during adsorption: A force field for alkanes in sodium-exchanged faujasites, J. Am. Chem. Soc. 126 (2004) 11377–11386.
[71] C. Janiak, A critical account on π–π stacking in metal complexes with aromatic nitrogen-containing ligands, J. Chem. Soc., Dalton Trans (2000) 3885–3896.
[72] C.R. Martinez, B.L. Iverson, Rethinking the term “pi-stacking”, Chem. Sci. 3 (2012) 2191–2201.
[73] K.S. Walton, A.R. Millward, D. Dubbeldam, H. Frost, J.J. Low, O.M. Yaghi, R.Q. Snurr, Understanding inflections and steps in carbon dioxide adsorption isotherms in metal-organic frameworks, J. Am. Chem. Soc. 130 (2008) 406–407.
[74] M.L. Waters, Aromatic interactions in model systems, Curr. Opin. Chem. Biol. 6 (2002) 736–741.
[75] C. Ge, J. Du, L. Zhao, L. Wang, Y. Liu, D. Li, Y. Yang, R. Zhou, Y. Zhao, Z. Chai,

Binding of blood proteins to carbon nanotubes reduces cytotoxicity, Proceedings of the National Academy of Sciences 108 (2011) 16968–16973.
[76] G. Zuo, W. Gu, H. Fang, R. Zhou, Carbon nanotube wins the competitive binding over proline-rich motif ligand on SH3 domain, The Journal of Physical Chemistry C 115 (2011) 12322–12328.
[77] S. Wallwork, Hydrogen-bond radii, Acta Crystallogr. 15 (1962) 758–759.
[78] V. Bolis, C. Busco, P. Ugliengo, Thermodynamic study of water adsorption in high-silica zeolites, J. Phys. Chem. B 110 (2006) 14849–14859.
[79] P. Boulet, L. Narasimhan, D. Berg'e-Lefranc, B. Kuchta, O. Schäf, R. Denoyel, Adsorption into the MFI zeolite of aromatic molecule of biological relevance. Investigations by Monte Carlo simulations, J. Mol. Model. 15 (2009) 573-579.
[80] E. Guvenc, M.G. Ahunbay, Adsorption of methyl tertiary butyl ether and trichloroethylene in MFI-type zeolites, J. Phys. Chem. C 116 (2012) 21836–21843.
[81] J. Reungoat, J.S. Pic, M.H. Manero, H. Debellefontaine, Adsorption of nitrobenzene from water onto high silica zeolites and regeneration by ozone, Sep. Sci. Technol. 42 (2007) 1447–1463.
[82] L. Damjanovic, V. Rakic, V. Rac, D. Stosic, A. Auroux, The investigation of phenol removal from aqueous solutions by zeolites as solid adsorbents, J. Hazard. Mater. 184 (2010) 477–484.
[83] R. Gonzalez-Olmos, F.-D. Kopinke, K. Mackenzie, A. Georgi, Hydrophobic Fe-zeolites for removal of MTBE from water by combination of adsorption and oxidation, Environ. Sci. Technol. 47 (2013) 2353–2360.